Ultrafast Saturable Absorption of Two-Dimensional MoS_2 Nanosheets

Kangpeng Wang,[†] Jun Wang,[†,*] Jintai Fan,[†] Mustafa Lotya,[‡] Arlene O'Neill,[‡] Daniel Fox,[‡] Yanyan Feng,[†] Xiaoyan Zhang,[†] Benxue Jiang,[†] Quanzhong Zhao,[§] Hongzhou Zhang,[‡] Jonathan N. Coleman,[‡] Long Zhang,[†,*] and Werner Josef Blau[†,‡,*]

[†]Key Laboratory of Materials for High-Power Laser, Shanghai Institute of Optics and Fine Mechanics, Chinese Academy of Sciences, Shanghai 201800, China, [‡]School of Physics and the Centre for Research on Adaptive Nanostructures and Nanodevices (CRANN), Trinity College Dublin, Dublin 2, Ireland, and [§]The State Key Laboratory of High Field Laser Physics, Shanghai Institute of Optics and Fine Mechanics, Chinese Academy of Sciences, Shanghai 201800, China

ABSTRACT Employing high-yield production of layered materials by liquid-phase exfoliation, molybdenum disulfide (MoS_2) dispersions with large populations of single and few layers were prepared. Electron microscopy verified the high quality of the two-dimensional MoS_2 nanostructures. Atomic force microscopy analysis revealed that ~39% of the MoS_2 flakes had thicknesses of less than 5 nm. Linewidth and frequency difference of the E^1_{2g} and A_{1g} Raman modes confirmed the effective reduction of flake thicknesses from the bulk MoS_2 to the dispersions. Ultrafast nonlinear optical (NLO) properties were investigated using an open-aperture Z-scan technique. All experiments were performed using 100 fs pulses at 800 nm from a mode-locked Ti:sapphire laser. The MoS_2 nanosheets exhibited significant saturable absorption (SA) for the femtosecond pulses, resulting in the third-order NLO susceptibility $\mathrm{Im}\chi^{(3)} \sim 10^{-15}$ esu, figure of merit $\sim 10^{-15}$ esu cm, and free-carrier absorption cross section $\sim 10^{-17}$ cm^2. Induced free carrier density and the relaxation time were estimated to be $\sim 10^{16}$ cm^{-3} and ~30 fs, respectively. At the same excitation condition, the MoS_2 dispersions show better SA response than the graphene dispersions.

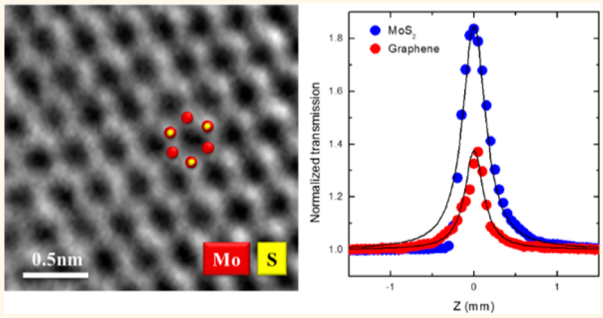

KEYWORDS: 2D nanomaterials · MoS_2 · transition metal dichalcogenides · ultrafast · nonlinear optics · Z-scan · saturable absorption

Research on graphene highlights a new nanomaterial with excellent physical and chemical properties. Most importantly, the material revolutionized the traditional ideology of nanoscience and nanotechnology and opened up a door to a new two-dimensional (2D) nanosystem.[1−3] Following the same vein on graphene study, researchers have started the exploration of graphene analogues—materials comprising stacked atomic or molecular layers.[4−7] Strong covalent bonds in layers and weak van der Waals interaction between layers allow the graphene analogues to form a robust 2D nanostructure. Layered molybdenum disulfide (MoS_2) is one of the typical graphene analogues.[8,9] Owing to the specific 2D confinement of electron motion and the absence of interlayer perturbation, the MoS_2 monolayer possesses a direct band gap and shows dramatic improvement in photoluminescence quantum efficiency by a factor of 10^4 in comparison with the bulk counterpart.[10−14] The remarkable physical properties of the layered semiconductor nanomaterial inject new opportunities in the field of photonics and optoelectronics.[2,3,5]

For the sake of the development of viable photonic devices, investigation of the nonlinear and ultrafast optical properties of the 2D nanomaterials, such as nonlinear susceptibility, nonlinear refraction and absorption, carrier relaxation lifetime, *etc.*, is undoubtedly important. Regardless of the design and fabrication processes, these basic photonic coefficients determine primarily the performance of the nanophotonic devices. In this work, we studied for the first time, to the best of our knowledge, the ultrafast nonlinear optical (NLO) property of 2D MoS_2 nanosheets in dispersions. Using the high-yield liquid-phase exfoliation (LPE) technique,[9,15] a series of dispersions with large populations of monolayer and few-layer MoS_2 were prepared in *N*-methylpyrrolidone (NMP), *N*-vinylpyrrolidinone (NVP), and cyclohexylpyrrolidinone (CHP).

* Address correspondence to jwang@siom.ac.cn, lzhang@siom.ac.cn, wblau@tcd.ie.

Received for review July 26, 2013 and accepted October 3, 2013.

Published online October 03, 2013
10.1021/nn403886t

Electronic microscopy and atomic force microscopy (AFM) verified the high quality of the 2D nanostructures. Linewidth and frequency difference of the E^1_{2g} and A_{1g} Raman modes confirmed the effective reduction of flake thicknesses from the bulk MoS_2 to the dispersions. The MoS_2 nanosheets exhibited significant saturable absorption (SA) for femtosecond pulses at 800 nm, resulting in the third-order NLO susceptibility $Im\chi^{(3)} \sim 10^{-15}$ esu and free-carrier absorption (FCA) cross section $\sim 10^{-17}$ cm^2. The results imply that the layered transition metal dichalcogenides (TMDs) are promising 2D nanomaterials for nanophotonic devices, such as saturable absorbers, optical switches, *etc.*

RESULTS AND DISCUSSION

Our previous experimental and theoretical analyses reveal that the surface energy of the layered materials should match very well with that of the dispersant, resulting in a minimal energy cost of overcoming the van der Waals forces between two adjacent monolayers, hence effective exfoliation to single or few layers.[9,16−18] In this work, three different organic solvents, namely, NMP, NVP, and CHP, were chosen to disperse MoS_2. Figure 1a shows photographs of the MoS_2 dispersions being treated in NMP at different stages. The dark color of the samples after a high-power sonication process for 60 min implies a stable dispersion with high concentration. After sonication, the dispersions were allowed to settle for ~24 h before centrifuging. The top two-thirds of the dispersions was collected by pipet after the centrifugation at 1500 rpm for 90 min. As a result of the removal of large sedimentations, the stability as well as the transmission of the extracted dispersions improves significantly. Using scanning transmission electron microscopy (STEM), we can find that the initial dispersions without sonication treatment consist of a number of MoS_2 platelets with lateral thickness of a few micrometers (Figure 1b). After high-power sonication treatment, the MoS_2 platelets were effectively exfoliated to 2D nanoflakes with a thickness of a few nanometers (Figure 1c). Meanwhile, the size of the objects was reduced from several micrometers to hundreds of nanometers. The MoS_2 used in this work has two layers per unit cell stacked in hexagonal symmetry (2H). As shown in Figure 1d, graphene-like hexagonal structure was observed from the MoS_2 nanosheets by high-resolution TEM. By the analysis of intensity profile across the dotted line in Figure 1d, a significant variation in intensity between neighboring atoms can be observed. Due to the ABAB stacking sequence of the 2H polytype, the image intensity between neighboring atoms would have no difference in contrast for the sample of more than two layers.[9] Therefore, the strong intensity difference shown in Figure 1e suggests the MoS_2 sheet in Figure 1d to be monolayer.

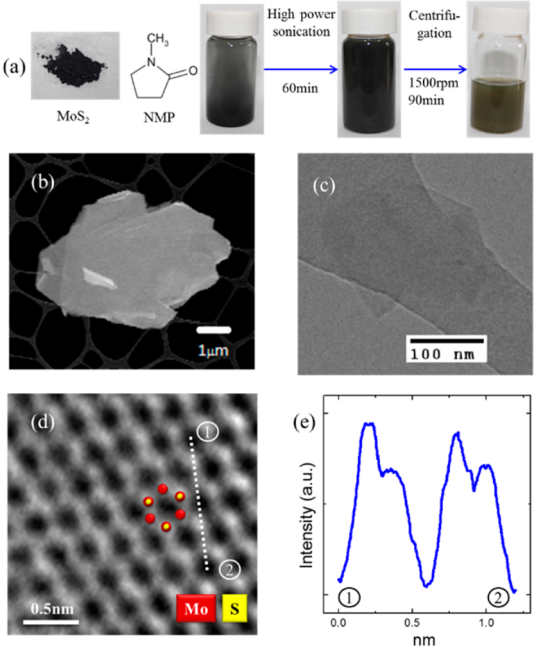

Figure 1. (a) Photographs of the MoS_2 dispersions being processed at different stages. Electronic microscopic images of the MoS_2 flakes (b) before and (c) after the sonication treatment. (d) High-resolution TEM image and (e) intensity distribution along the dotted line in (d) for a MoS_2 nanosheet. The samples for TEM analysis were prepared by dropping a few milliliters of each dispersion on copper holey carbon grids (mesh size 400).

The status of the dispersed MoS_2 nanosheets was investigated in detail by using STEM. A large number of well-exfoliated nanoflakes can be seen readily. STEM image and lateral profile of a MoS_2 nanosheet are given in Figure 2a,b. The intensity of each pixel along the lines ①−② and ③−④ in Figure 2a is proportional to the relative height of the flake. Unlike the dispersed graphene flakes that have scrolled or folded edges,[19] the MoS_2 flakes exhibit sharp edges with relatively regular geometrical shapes, implying a rigid crystal structure and stiff mechanical property in comparison with graphene flakes. Consistent with what we obtained before,[9] the average size of the MoS_2 flakes is in the hundreds of nanometers, revealing a typical 2D nanostructure. In addition, it can be seen in Figure 2b that the lateral profiles of the nanoflakes show clearly multiple layered structures. The thickness ratios of the layers keep approximately integers (*i.e.*, layer A:B:C:D ≈ 1:4:3:2). The integral ratios imply that the thinnest layer A has very good chance of being monolayer. Suppose that layer A was a double layer, it has only a 12.5% possibility that layers B, C, and D happen to be even number layers.

To determine size as well as thickness of the MoS_2 flakes, an atomic force microscopy (AFM) measurement was carried out. The AFM samples were prepared by casting a few drops of the dispersions on precleaned Si substrates, followed by a high-temperature vacuum treatment to get rid of the residual solvents. As shown in Figure 2c, large quantities of deposited MoS_2

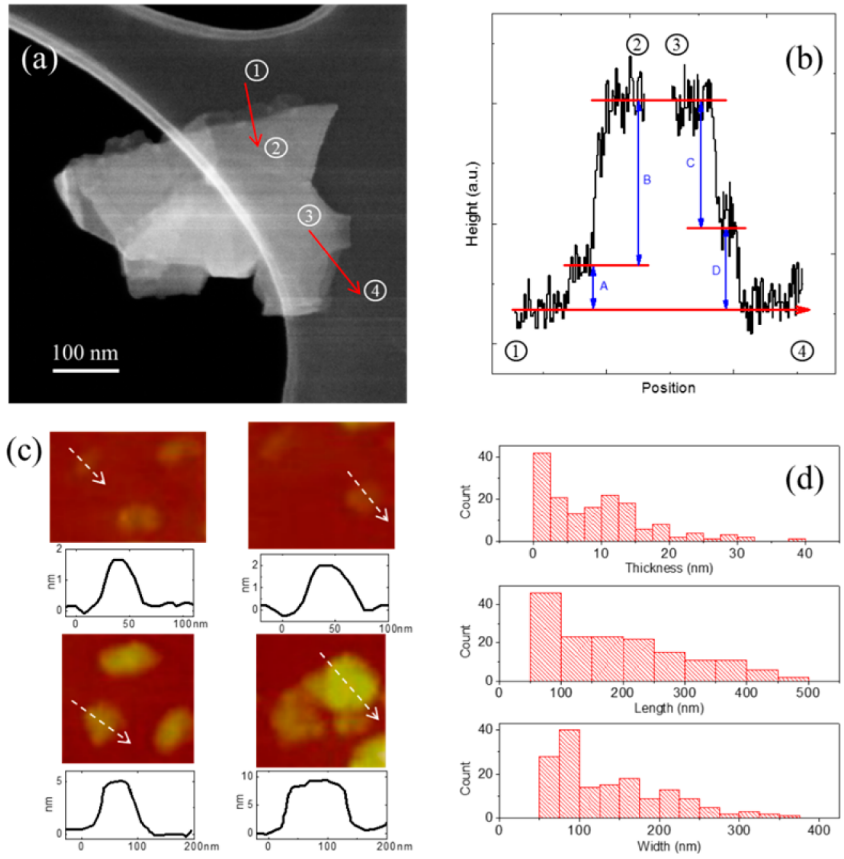

Figure 2. (a) STEM image and (b) lateral profile of a MoS_2 nanosheet. (c) Typical AFM images, thickness profiles and (d) histograms of thicknesses, lengths, and widths of the deposited MoS_2 nanosheets.

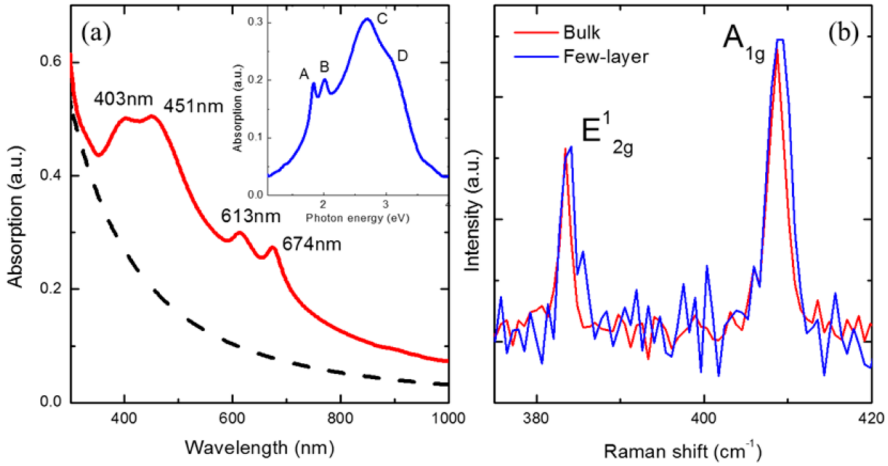

Figure 3. (a) Absorption spectrum of the MoS_2 dispersions. The dashed line is the calculated scattering background. Inset: absorption without the scattering. (b) Raman spectra of the few-layer and bulk MoS_2.

nanoflakes can be observed by AFM. Figure 2d illustrates histograms of thicknesses, lengths, and widths of the deposited MoS_2 flakes. Statistical analysis reveals that ~39% of the flakes out of a total of 160 objects counted had thicknesses of less than 5 nm. Taking into account the aggregation effect occurring during the deposition and drying processes of preparing AFM samples, we believe that the thicknesses of the MoS_2 flakes in dispersions were much smaller than the statistical values in Figure 2d. The probability of deposited flakes with lengths less than 200 nm was ~58%, and the lengths of almost all observed flakes were less than 450 nm. Correspondingly, ~43% of flakes had widths <100 nm, and ~78% of flakes with widths <200 nm. Moreover, it was found that the bigger flakes tended to be thicker than the smaller flakes.

An absorption spectrum of the MoS_2 dispersions is illustrated in Figure 3a. The four characteristic

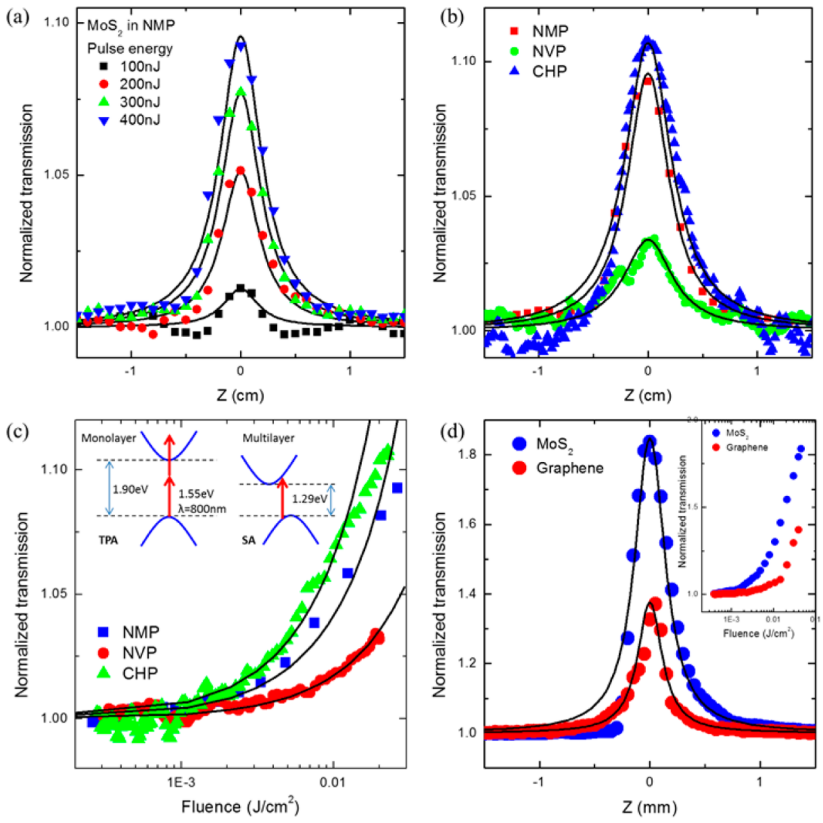

Figure 4. Open-aperture Z-scans of the MoS_2 dispersions under the excitation of 100 fs pulses at 800 nm (a) with different pulse energies and (b) in different solvents. (c) Normalized transmission as a function of fluence for the three dispersions. Inset: illustrations of TPA and SA. (d) Z-scan results for the MoS_2 (T = 34.4%) and graphene (T = 16.5%) dispersions. Inset: normalized transmission as a function of fluence. The solid lines are the theoretical fit curves from model 1 (a,b,d) and model 3 (c).

absorption peaks located at 600−700 nm and 400−450 nm regions coincide with the general features of TMDs with trigonal prismatic coordination,[20,21] implying the MoS_2 nanosheets 2H polytype. The absorption peaks correspond to four different electronic transitions, termed as A, B, C, and D, in the band structure of MoS_2. For clarity, the Mie scattering induced background was subtracted in the inset of Figure 3a. The scattering induced extinction, as illustrated by the dashed line in Figure 3a, was estimated by the empirical formula, scattering $\propto \lambda^{-2.35}$.[9] The dual peaks at 600−700 nm originate from A and B, the interband excitonic transitions at the K point of the 2D Brillouin zone of MoS_2. The separation of A and B is regarded as being due to the spin−orbit splitting of transitions at K.[20,21] The absorption peaks at 400−450 nm (*i.e.*, C and D) arise from the transitions between the higher density of state regions.[20,21]

Raman spectroscopy was employed to confirm the atomic structural arrangement of MoS_2. The study was carried out using a Jobin Yvon LabRam 1B Raman spectrometer with an Ar laser at 514 nm. As shown in Figure 3b, the Raman spectra of the deposited MoS_2 flakes exhibit the distinct Raman fingerprint of the 2H-MoS_2 crystal with no evidence of structural distortion.[22] The characteristic bands at 384.2 and 408.7 cm^{-1} are assigned as the in-plane (E^1_{2g}) and out-of-plane (A_{1g}) vibrational modes. For the MoS_2 with 1T polytype, the spectrum does not show the E_{2g} Raman mode. The layered 2H-MoS_2 exhibits anomalous lattice vibrations; that is, the frequency of the A_{1g} mode increases and that of the E^1_{2g} mode decreases along with the increase of the number of monolayers in a flake.[22] In addition, it has been shown that the frequency difference of the two modes can be used to distinguish the few-layer MoS_2 and its bulk counterpart as well as to estimate the number of monolayers.[22] In this work, a mean frequency difference of ∼24.5 cm^{-1} was obtained for the few-layer flakes, implying an average thickness of ∼5−6 monolayers, that is, ∼4 nm (∼0.65 nm for each monolayer). In contrast, the mean difference for the bulk MoS_2 was increased to ∼25.2 cm^{-1}. Whereas the difference of the frequency differences of the few-layer and bulk MoS_2 (0.7 cm^{-1}) is close to the resolution of the Raman spectrometer, the broadening of the linewidths of the E^1_{2g} band (∼2.0 cm^{-1}) and A_{1g} band (∼3.2 cm^{-1}) for the few-layer flakes in comparison with those of the bulk MoS_2 (*i.e.*, 1.4 cm^{-1} for E^1_{2g} and 2.5 cm^{-1} for A_{1g}) verifies the significant reduction of the flake thicknesses from the bulk MoS_2 to the dispersed samples.[22] Again, it must be pointed out that the inevitable aggregation effect of

the layered nanoflakes that occurred in the Raman samples' preparation procedure restricts certainly the accuracy of the Raman spectra in Figure 3b to reflect the real status of the flakes in dispersions.

An open-aperture Z-scan system in conjunction with a mode-locked Ti:sapphire laser operating at 800 nm, 100 fs pulses, with 1 kHz repetition rate was employed to study the ultrafast NLO behavior of the MoS_2 dispersions.[19,23] As shown in Figure 4a, the NLO response of MoS_2 nanosheets took place in the NMP dispersions when the excitation energy was increased up to 100 nJ/pulse, corresponding to an estimated on-focus intensity of ~65.8 GW/cm^2 and a fluence of ~6.6 mJ/cm^2. At the excitation energies of larger than 200 nJ/pulse (~131.6 GW/cm^2), the MoS_2 dispersions exhibit obvious SA response; that is, the total transmission increases as the intensity of the incident beam increased ($z \rightarrow 0$). That is to say, the MoS_2 nanosheets can effectively suppress low intensity light but allow high pass for higher intensity light. The absorption saturation for femtosecond pulses in the NIR region implies that the MoS_2 nanosheets could serve as ultrafast nonlinear saturable absorber, a passive mode-locking element for ultrashort pulsed lasers.[24−27]

The monolayer MoS_2 is a direct semiconductor with a band gap of ~1.9 eV, while the multilayer MoS_2 is an indirect semiconductor with a narrower band gap of ~1.2 eV.[11,12] For the photons with an energy of 1.55 eV (λ = 800 nm), the multilayer MoS_2 is able to be excited with one photon. In contrast, the monolayer can only be excited by absorbing two photons simultaneously. When excited with a high intensity femtosecond laser beam at 800 nm, the monolayer and multilayer MoS_2 possess two-photon absorption (TPA) and absorption saturation, respectively, as illustrated in the inset of Figure 4c. Therefore, the strong SA in Figure 4 originates from the multilayer nanosheets in the MoS_2 dispersions. It should be pointed out that TPA of the MoS_2 monolayer will result in a decrease of the transmission, as opposed to the increase of the transmission around the focal point in the Z-scan experiment.[28]

According to the NLO theory, we write the propagation equation in the MoS_2 dispersions in the form of (model 1)

$$\frac{dI}{dz'} = -\alpha(I)I \quad (1)$$

where z' is the propagation distance in the samples, and the total absorption $\alpha(I)$ consists of a linear absorption coefficient α_0 and a nonlinear absorption coefficient α_{NL}

$$\alpha(I) = \alpha_0 + \alpha_{NL}I \quad (2)$$

In this experiment, we did not observe any clear nonlinear response from the dispersant solvents. The contribution of α_{NL} only comes from the nonlinear absorption of the MoS_2 nanosheets alone. By fitting the Z-scan data in Figure 4a using eqs 1 and 2, we obtained an average value of $\alpha_{NL} \sim -(4.60 \pm 0.27) \times 10^{-3}$ cm/GW. In addition, the on-focus beam radius was determined to be ~23.7 μm by fitting the experimental data. The imaginary part of the third-order NLO susceptibility, Im$\chi^{(3)}$, is directly related to α_{NL}

$$\mathrm{Im}\chi^{(3)} = \left[\frac{10^{-7}c\lambda n^2}{96\pi^2}\right]\alpha_{NL} \quad (3)$$

where c is the speed of light, λ is the wavelength of the incident light, and n is the refractive index. The figure of merit (FOM) for the third-order optical nonlinearity is defined as FOM = $|\mathrm{Im}\chi^{(3)}/\alpha_0|$, where $\alpha_0 \sim 2.37$ cm^{-1} for the NMP dispersions in Figure 4a. Therefore, Im$\chi^{(3)}$ and FOM for the MoS_2 nanosheets in NMP can be calculated as $-(2.52 \pm 0.15) \times 10^{-15}$ esu and $\sim(1.06 \pm 0.06) \times 10^{-15}$ esu cm, respectively. The value of FOM for the 2D MoS_2 is comparable with some other SA nanomaterials, such as graphene $\sim 5 \times 10^{-15}$ esu cm,[29] graphene oxide $\sim 4.2 \times 10^{-15}$ esu cm,[29] reduced graphene oxide $\sim 0.36 \times 10^{-15}$ esu cm,[30] $AgInSe_2$ nanorods $\sim 8 \times 10^{-15}$ esu cm,[31] and Au nanorods $\sim 0.88 \times 10^{-15}$ esu cm.[32] However, one should not omit the difference of the experimental conditions, such as wavelength, pulse width, repetition rate, *etc.*, in the above works. For the sake of a convincing comparison, we carried out the Z-scan measurements for graphene dispersions prepared by the similar liquid exfoliation.[15,19] As shown in Figure 4d, the MoS_2 dispersions exhibit much stronger SA response than the graphene dispersions. Taking into account the linear absorbance, we determined Im$\chi^{(3)}$ and FOM for MoS_2 to be -1.56×10^{-14} esu and $\sim 1.47 \times 10^{-15}$ esu cm, respectively, while those for graphene to be -8.14×10^{-15} esu and 4.52×10^{-16} esu cm, respectively. It can be expected that the MoS_2 nanosheets would possess much larger SA response at its resonant band at 400−700 nm.

For a system in which SA and TPA coexist, we can also describe $\alpha(I)$ in eq 1 with the form of (model 2)

$$\alpha(I) = \frac{\alpha_0}{1 + I/I_s} + \beta I \quad (4)$$

where I_s is the saturation intensity and β is the TPA coefficient. The first term on the right-hand side in eq 4 stands for SA, while the second term stands for TPA. From the fitting of Z-scan data in Figure 4a using eqs 1 and 4, we noticed that the TPA coefficient β has to be close to zero for the best fitting, implying that the contribution of the monolayer MoS_2, which is mainly attributed to TPA, was negligible. Overall, the model agrees quite well with the Z-scan results by choosing parameters $I_s \sim 413 \pm 24$ GW/cm^2. The saturation intensity combined with the excited state cross section can be utilized to estimate the relaxation time of the charge carriers in MoS_2.

TABLE 1. Linear and NLO Parameters of the MoS_2 Dispersions Excited in the Femtosecond Region

materials	T (%)	α_0 (cm^{-1})	α_{NL} (cm/GW)	$Im\chi^{(3)}$ (esu, $\times 10^{-15}$)	FOM (esu cm, $\times 10^{-15}$)	I_s (GW/cm^2)	σ_{FCA} (cm^2, $\times 10^{-17}$)	τ (fs)	N_0 (cm^3, $\times 10^{16}$)
MoS_2/NMP	78.9	2.37	$-(4.60 \pm 0.27) \times 10^{-3}$	$-(2.52 \pm 0.15)$	1.06 ± 0.06	413 ± 24	$-(1.85 \pm 0.10)$	32.54	5.65
MoS_2/NVP	84.7	1.66	$-(1.78 \pm 0.02) \times 10^{-3}$	$-(1.03 \pm 0.01)$	0.62 ± 0.01	833 ± 55	$-(1.10 \pm 0.10)$	27.13	3.68
MoS_2/CHP	75.2	2.85	$-(5.80 \pm 0.33) \times 10^{-3}$	$-(3.30 \pm 0.19)$	1.16 ± 0.07	405 ± 50	$-(1.95 \pm 0.05)$	31.48	6.76

In addition, we studied the nonlinear absorption of MoS_2 nanosheets dispersed in three different organic solvents (*i.e.*, NMP, NVP, and CHP). As shown in Figure 4b, significant ultrafast SA responses were observed readily from all these three dispersions. At the same incident energies, the CHP and NMP dispersions exhibited better SA response than the NVP dispersions. All NLO fitting parameters are summarized in Table 1. Due to the different linear absorbances as well as concentrations, the MoS_2 nanosheets in CHP have the largest $Im\chi^{(3)} \sim -(3.30 \pm 0.19) \times 10^{-15}$ esu and the smallest saturation intensity $I_s \sim 405 \pm 50$ GW/cm^2. In contrast, the NLO response of the NVP dispersions was inferior in comparison with the other two dispersions. The NMP and CHP dispersions show comparable value of FOM $\sim 1.1 \times 10^{-15}$ esu cm. Overall, the layered MoS_2 flakes retain their high nonlinear performance in different solvents.

Since the layered MoS_2 is a kind of semiconductor, we consider that the ultrafast nonlinear absorption of the MoS_2 dispersions in the NIR region originated from one-photon induced FCA. There is a compact model (model 3) related to the normalized transmission T and the peak incident fluence F_0[33]

$$T = \left(\frac{F_c}{F_0}\right)\ln\left(1+\frac{F_0}{F_c}\right) \quad (5)$$

where F_c is defined as a critical fluence $F_c = (2\hbar\omega)/[\sigma_{FCA}(1 - e^{-\alpha_0 L})]'$ where σ_{FCA} is the FCA cross section, α_0 is still the linear absorption coefficient, and $L = 0.1$ cm is the path length of the samples. The experimental data of T as a function of F_0 were converted directly from the Z-scan results. The σ_{FCA} can be estimated by fitting the data with eq 5. As shown in Figure 4c, the theoretical curves agree very well with the experiment when σ_{FCA} was set to be $-(1.85 \pm 0.10) \times 10^{-17}$, $-(1.10 \pm 0.10) \times 10^{-17}$, and $-(1.95 \pm 0.05) \times 10^{-17}$ cm^2 for the NMP, NVP, and CHP dispersions, respectively. With σ_{FCA}, the relaxation time of the excited states τ can be estimated by using $I_s = (h\nu)/(\alpha_{FCA}\tau')$, where the saturation intensity I_s comes from the Z-scan curve fitting by using eq 4. The MoS_2 nanosheets in the three different dispersions have the similar relaxation time of ~30 fs (see Table 1). It should be pointed out that the relaxation time τ here corresponds to the intraband transitions of the excited free carriers. In contrast, the lifetime of interband transitions was measured to be on the picosecond time scale for the monolayer or few-layer MoS_2.[34,35] The ultrafast relaxation implies that the 2D MoS_2 is able to serve as a saturable absorber for mode-locked ultrafast lasers, like single-walled carbon nanotubes[36] and graphene.[24,25]

Under the FCA model, the total absorption at a certain on-focus intensity I_0 has the form of

$$\alpha(I_0) = \alpha_0 + \sigma_{FCA}N_0 \quad (6)$$

where N_0 stands for the induced instantaneous free carrier density at I_0 and can be calculated using the equation $N_0 = (\alpha_0 F_0)/(\hbar\omega)$. With regard to Figure 4c, the fluence F_0 corresponding to the onset of SA is $\sim 1 \times 10^{-3}$ J cm^{-2}. We therefore can estimate an induced carrier density in the CHP dispersions of $\sim 1.14 \times 10^{16}$ cm^{-3}. On the other hand, N_0 can also be estimated by equaling eq 6 to eq 2, which gives $N_0 \sim 6.76 \times 10^{16}$ cm^{-3} for the same dispersions. Good agreement of N_0 from the two different estimations implies the validity of the estimated σ_{FCA} in Table 1. It should be mentioned that the magnitude of the carrier density N_0 estimated in this work is consistent with that deduced by the electrical method, in which the MoS_2 nanosheets were prepared by the LPE technique, as well.[37] In addition, it is worth noticing that the ratios of the estimated N_0 for the three dispersions at the same excitation condition is $N_{NMP}/N_{NVP}/N_{CHP}$ = 1.5:1.0:1.8. The concentration ratios of MoS_2 nanosheets in the three dispersions can be roughly deduced from their linear absorbances $C_{NMP}/C_{NVP}/C_{CHP}$ = 1.4:1.0:1.7. The carrier density ratios follow quite well with the concentration ratios.

Overall, the Z-scan data in Figure 4 have been analyzed with three different models. The mutual complementary models give a series of NLO parameters for the 2D MoS_2 nanosheets. The imaginary part of the third-order NLO susceptibility $Im\chi^{(3)}$ as well as the NLO absorption coefficient was obtained by the nonlinear absorption model (model 1). The saturation intensity I_s and the FCA cross section σ_{FCA} were deduced by the SA model (model 2) and the FCA model (model 3), respectively. The induced instantaneous free carrier density and the relaxation time of the excited states were estimated, as well.

CONCLUSIONS

In conclusion, a series of dispersions with large populations of high-quality monolayer and few-layer MoS_2 nanosheets were prepared using the LPE technique. The MoS_2 nanosheets exhibited strong SA for the femtosecond pulses at 800 nm. $Im\chi^{(3)} \sim 10^{-15}$ esu, FOM $\sim 10^{-15}$ esu cm, and $\sigma_{FCA} \sim 10^{-17}$ cm^2 were obtained for the MoS_2 nanosheets. The induced free

carrier density and the relaxation time were estimated to be $\sim 10^{16}$ cm^{-3} and $\sim$30 fs, respectively. At the same excitation condition, the MoS_2 dispersions show better SA response than the graphene dispersions. The significant ultrafast NLO properties of the layered MoS_2 imply a huge potential in the development of nanophotonic devices, such as mode-lockers, optical switches, *etc.* It should be pointed out that the value of the exfoliated MoS_2 dispersions consists of their high expandability. Starting with the dispersions, one can readily prepare derivatives with various forms, such as filtrated neat films, polymer composites, functionalized composites, *etc.*, to satisfy requirements for different photonic devices and applications.

EXPERIMENTAL SECTION

MoS_2 Dispersions. All chemicals used in the work were purchased from Sigma-Aldrich. The MoS_2 powders were dispersed in NMP, NVP, and CHP with a concentration of 7.5 mg/mL. Initial MoS_2 dispersions were produced by sonication using a point probe (flathead sonic tip) for 60 min with a power output of 285 W, followed by 24 h standing and centrifugation at 1500 rpm for 90 min. After centrifugation, the top two-thirds of the dispersions was gently extracted by pipetting.

Z-Scan. An open-aperture Z-scan system was used to study the ultrafast NLO behavior of the MoS_2 and graphene dispersions. This measures the total transmittance through a sample as a function of incident laser intensity, while the sample is sequentially moved through the focus of a lens (along the *z*-axis). The optical arrangement was analogous to that used in our previous experiments in measuring NLO response of carbon nanotube and graphene dispersions.[19,23]

Conflict of Interest: The authors declare no competing financial interest.

Acknowledgment. J.W. thanks the 100-Talent Program of Chinese Academy of Sciences, the National Natural Science Foundation of China (NSFC, No. 61178007), and Science and Technology Commission of Shanghai Municipality (STCSM Nano Project, No. 11 nm0502400, Shanghai Pujiang Program 12PJ1409400) for financial support. L.Z. thanks the STCSM Excellent Academic Leader of Shanghai (No. 10XD1404600) and the Shanghai Natural Science Foundation (No. 11ZR1441500) for financial support. J.N.C. is supported by the ERC Grant SEMANTICS. W.J.B. gratefully acknowledges a visiting professorship for international scientists from the Chinese Academy of Sciences. His contribution towards this publication has also emanated from research supported in part by a research grant from Science Foundation Ireland (SFI) under Grant Number 12/IA/1306. X.Y.Z. thanks the NSFC No. 51302285 for financial support.

REFERENCES AND NOTES

1. Geim, A. K.; Novoselov, K. S. The Rise of Graphene. *Nat. Mater.* **2007**, *6*, 183–191.
2. Bonaccorso, F.; Sun, Z.; Hasan, T.; Ferrari, A. C. Graphene Photonics and Optoelectronics. *Nat. Photonics* **2010**, *4*, 611–622.
3. Loh, K. P.; Bao, Q. L.; Eda, G.; Chhowalla, M. Graphene Oxide as a Chemically Tunable Platform for Optical Applications. *Nat. Chem.* **2010**, *2*, 1015–1024.
4. Mas-Balleste, R.; Gomez-Navarro, C.; Gomez-Herrero, J.; Zamora, F. 2D Materials: To Graphene and Beyond. *Nanoscale* **2011**, *3*, 20–30.
5. Wang, Q. H.; Kalantar-Zadeh, K.; Kis, A.; Coleman, J. N.; Strano, M. S. Electronics and Optoelectronics of Two-Dimensional Transition Metal Dichalcogenides. *Nat. Nanotechnol.* **2012**, *7*, 699–712.
6. Butler, S. Z.; Hollen, S. M.; Cao, L.; Cui, Y.; Gupta, J. A.; Gutiérrez, H. R.; Heinz, T. F.; Hong, S. S.; Huang, J.; Ismach, A. F.; *et al.* Progress, Challenges, and Opportunities in Two-Dimensional Materials Beyond Graphene. *ACS Nano* **2013**, *7*, 2898–2926.
7. Nicolosi, V.; Chhowalla, M.; Kanatzidis, M. G.; Strano, M. S.; Coleman, J. N. Liquid Exfoliation of Layered Materials. *Science* **2013**, *340*, 1226419.
8. Ramakrishna Matte, H. S. S.; Gomathi, A.; Manna, A. K.; Late, D. J.; Datta, R.; Pati, S. K.; Rao, C. N. R. MoS_2 and WS_2 Analogues of Graphene. *Angew. Chem., Int. Ed.* **2010**, *49*, 4059–4062.
9. Coleman, J. N.; Lotya, M.; O'Neill, A.; Bergin, S. D.; King, P. J.; Khan, U.; Young, K.; Gaucher, A.; De, S.; Smith, R. J.; *et al.* Two-Dimensional Nanosheets Produced by Liquid Exfoliation of Layered Materials. *Science* **2011**, *331*, 568–571.
10. Radisavljevic, B.; Radenovic, A.; Brivio, J.; Giacometti, V.; Kis, A. Single-Layer MoS_2 Transistors. *Nat. Nanotechnol.* **2011**, *6*, 147–150.
11. Mak, K. F.; Lee, C.; Hone, J.; Shan, J.; Heinz, T. F. Atomically Thin MoS_2: A New Direct-Gap Semiconductor. *Phys. Rev. Lett.* **2010**, *105*, 136805.
12. Splendiani, A.; Sun, L.; Zhang, Y.; Li, T.; Kim, J.; Chim, C.-Y.; Galli, G.; Wang, F. Emerging Photoluminescence in Monolayer MoS_2. *Nano Lett.* **2010**, *10*, 1271–1275.
13. Eda, G.; Yamaguchi, H.; Voiry, D.; Fujita, T.; Chen, M.; Chhowalla, M. Photoluminescence from Chemically Exfoliated MoS_2. *Nano Lett.* **2011**, *11*, 5111–5116.
14. Radisavljevic, B.; Kis, A. Mobility Engineering and a Metal-Insulator Transition in Monolayer MoS_2. *Nat. Mater.* **2013**, *12*, 815–820.
15. Hernandez, Y.; Nicolosi, V.; Lotya, M.; Blighe, F. M.; Sun, Z.; De, S.; McGovern, I. T.; Holland, B.; Byrne, M.; Gun'Ko, Y. K.; *et al.* High-Yield Production of Graphene by Liquid-Phase Exfoliation of Graphite. *Nat. Nanotechnol.* **2008**, *3*, 563–568.
16. Cunningham, G.; Lotya, M.; Cucinotta, C. S.; Sanvito, S.; Bergin, S. D.; Menzel, R.; Shaffer, M. S. P.; Coleman, J. N. Solvent Exfoliation of Transition Metal Dichalcogenides: Dispersibility of Exfoliated Nanosheets Varies Only Weakly between Compounds. *ACS Nano* **2012**, *6*, 3468–3480.
17. O'Neill, A.; Khan, U.; Coleman, J. N. Preparation of High Concentration Dispersions of Exfoliated MoS_2 with Increased Flake Size. *Chem. Mater.* **2012**, *24*, 2414–2421.
18. Coleman, J. N. Liquid-Phase Exfoliation of Nanotubes and Graphene. *Adv. Funct. Mater.* **2009**, *19*, 3680–3695.
19. Wang, J.; Hernandez, Y.; Lotya, M.; Coleman, J. N.; Blau, W. J. Broadband Nonlinear Optical Response of Graphene Dispersions. *Adv. Mater.* **2009**, *21*, 2430–2435.
20. Beal, A. R.; Knights, J. C.; Liang, W. Y. Transmission Spectra of Some Transition Metal Dichalcogenides. II. Group VIA: Trigonal Prismatic Coordination. *J. Phys. C: Solid State Phys.* **1972**, *5*, 3540.
21. Bromley, R. A.; Murray, R. B.; Yoffe, A. D. The Band Structures of Some Transition Metal Dichalcogenides. III. Group VIA: Trigonal Prism Materials. *J. Phys. C: Solid State Phys.* **1972**, *5*, 759.
22. Lee, C.; Yan, H.; Brus, L. E.; Heinz, T. F.; Hone, J.; Ryu, S. Anomalous Lattice Vibrations of Single- and Few-Layer MoS_2. *ACS Nano* **2010**, *4*, 2695–2700.
23. Wang, J.; Früchtl, D.; Sun, Z.; Coleman, J. N.; Blau, W. J. Control of Optical Limiting of Carbon Nanotube Dispersions by Changing Solvent Parameters. *J. Phys. Chem. C* **2010**, *114*, 6148–6156.
24. Bao, Q.; Zhang, H.; Wang, Y.; Ni, Z.; Yan, Y.; Shen, Z. X.; Loh, K. P.; Tang, D. Y. Atomic-Layer Graphene as a Saturable

Absorber for Ultrafast Pulsed Lasers. *Adv. Funct. Mater.* **2009**, *19*, 3077–3083.
25. Sun, Z. P.; Hasan, T.; Torrisi, F.; Popa, D.; Privitera, G.; Wang, F. Q.; Bonaccorso, F.; Basko, D. M.; Ferrari, A. C. Graphene Mode-Locked Ultrafast Laser. *ACS Nano* **2010**, *4*, 803–810.
26. Wang, J.; Chen, Y.; Blau, W. J. Carbon Nanotubes and Nanotube Composites for Nonlinear Optical Devices. *J. Mater. Chem.* **2009**, *19*, 7425–7443.
27. Blau, W. J.; Wang, J. Optical Materials: Variety Pays off for Nanotubes. *Nat. Nanotechnol.* **2008**, *3*, 705–706.
28. Wang, J.; Blau, W. J. Inorganic and Hybrid Nanostructures for Optical Limiting. *J. Opt. A: Pure Appl. Opt.* **2009**, *11*, 024001.
29. Kumar, S.; Anija, M.; Kamaraju, N.; Vasu, K. S.; Subrahmanyam, K. S.; Sood, A. K.; Rao, C. N. R. Femtosecond Carrier Dynamics and Saturable Absorption in Graphene Suspensions. *Appl. Phys. Lett.* **2009**, *95*, 191911.
30. Kumar, S.; Kamaraju, N.; Vasu, K. S.; Nag, A.; Sood, A. K.; Rao, C. N. R. Graphene Analogue BCN: Femtosecond Nonlinear Optical Susceptibility and Hot Carrier Dynamics. *Chem. Phys. Lett.* **2010**, *499*, 152–157.
31. Elim, H. I.; Ji, W.; Ng, M. T.; Vittal, J. J. $AgInSe_2$ Nanorods: A Semiconducting Material for Saturable Absorber. *Appl. Phys. Lett.* **2007**, *90*, 033106.
32. Elim, H. I.; Yang, J.; Lee, J. Y.; Mi, J.; Ji, W. Observation of Saturable and Reverse-Saturable Absorption at Longitudinal Surface Plasmon Resonance in Gold Nanorods. *Appl. Phys. Lett.* **2006**, *88*, 083107.
33. Boggess, T. F.; Bohnert, K. M.; Mansour, K.; Moss, S. C.; Boyd, I. W.; Smirl, A. L. Simultaneous Measurement of the Two-Photon Coefficient and Free-Carrier Cross Section above the Bandgap of Crystalline Silicon. *IEEE J. Quantum Electron.* **1986**, *22*, 360–368.
34. Korn, T.; Heydrich, S.; Hirmer, M.; Schmutzler, J.; Schuller, C. Low-Temperature Photocarrier Dynamics in Monolayer MoS_2. *Appl. Phys. Lett.* **2011**, *99*, 102109.
35. Wang, R.; Ruzicka, B. A.; Kumar, N.; Bellus, M. Z.; Chiu, H.-Y.; Zhao, H. Ultrafast and Spatially Resolved Studies of Charge Carriers in Atomically Thin Molybdenum Disulfide. *Phys. Rev. B* **2012**, *86*, 045406.
36. Set, S. Y.; Yaguchi, H.; Tanaka, Y.; Jablonski, M. Ultrafast Fiber Pulsed Lasers Incorporating Carbon Nanotubes. *IEEE J. Sel. Top. Quantum Electron.* **2004**, *10*, 137–146.
37. Lee, K.; Kim, H.-Y.; Lotya, M.; Coleman, J. N.; Kim, G.-T.; Duesberg, G. S. Electrical Characteristics of Molybdenum Disulfide Flakes Produced by Liquid Exfoliation. *Adv. Mater.* **2011**, *23*, 4178–4182.